Anthropogenic-scale CO_2 degassing from the Central Atlantic Magmatic Province as a driver of the end-Triassic mass extinction

Capriolo, Manfredo; Mills, Benjamin J.W.; Newton, Robert J.; Dal Corso, Jacopo; Dunhill, Alexander M.; Wignall, Paul B.; Marzoli, Andrea

Anthropogenic-scale CO_2 degassing from the Central Atlantic Magmatic Province as a driver of the end-Triassic mass extinction

Manfredo Capriolo [a,b,*], Benjamin J.W. Mills [c], Robert J. Newton [c], Jacopo Dal Corso [d], Alexander M. Dunhill [c], Paul B. Wignall [c], Andrea Marzoli [e]

[a] *Department of Geosciences, University of Padova, Padova 35131, Italy*
[b] *Centre for Earth Evolution and Dynamics, University of Oslo, Oslo 0371, Norway*
[c] *School of Earth and Environment, University of Leeds, Leeds LS2 9JT, United Kingdom*
[d] *State Key Laboratory of Biogeology and Environmental Geology, China University of Geosciences, Wuhan 430074, China*
[e] *Department of Territory and Agro-Forestry Systems, University of Padova, Legnaro 35020, Italy*

A R T I C L E I N F O

A B S T R A C T

The climatic and environmental impact of exclusively volcanic CO_2 emissions is assessed during the main effusive phase of the Central Atlantic Magmatic Province (CAMP), which is synchronous with the end-Triassic mass extinction. CAMP volcanism occurred in brief and intense eruptive pulses each producing extensive basaltic lava flows. Here, CAMP volcanic CO_2 injections into the surface system are modelled using a biogeochemical box model for the carbon cycle. Our modelling shows that, even if positive feedback phenomena may be invoked to explain the carbon isotope excursions preserved in end-Triassic sedimentary records, intense and pulsed volcanic activity alone may have caused repeated temperature increases and pH drops, up to 5 °C and about 0.2 log units respectively. Hence, rapid and massive volcanic CO_2 emissions from CAMP, on a similar scale to current anthropogenic emissions, severely impacted on climate and environment at a global scale, leading to catastrophic biotic consequences.

1. Introduction

The synchrony in the Phanerozoic geological record between biotic crises and the emplacement of Large Igneous Provinces (LIPs) suggests volcanic degassing as the trigger of mass extinction-scale climatic and environmental disruption (e.g., Courtillot and Renne, 2003; Wignall, 2015; Bond and Grasby, 2017; Black et al., 2021). The Central Atlantic Magmatic Province (CAMP) is one of the most voluminous known LIPs, emplaced through brief and intense pulses (Marzoli et al., 1999, 2018, 2019; Knight et al., 2004), and coincides in time with the end-Triassic mass extinction (Marzoli et al., 2004; Schoene et al., 2010; Blackburn et al., 2013; Davies et al., 2017). The end-Triassic mass extinction, assumed to have occurred at about 201.564 ± 0.015 Ma (Ma = million years; Blackburn et al., 2013), is among the *Big 5*, the most severe mass extinction events during the Phanerozoic (Raup and Sepkoski Jr., 1982). With an estimated loss of 80% of marine invertebrate species (Hallam and Wignall, 1999), this event represents the single largest loss of modern fauna and the second largest loss of total biodiversity throughout Earth's history (Alroy, 2010), causing temporary but severe

changes to global marine ecosystem structure (McGhee Jr. et al., 2004; Dunhill et al., 2018a). Palynological and biostratigraphic evidence from both marine and continental sedimentary records indicates the occurrence of two distinct phases for the end-Triassic biotic crisis, separated by a recovery interval and likely driven by different volcanic phases of CAMP activity (Wignall and Atkinson, 2020; Lindström, 2021). The initial and most severe phase of the biological crisis occurred synchronously with the main phase of CAMP volcanism (Lindström, 2021). This coincidence strengthens the causality relationship between the volcanic activity and the biotic crisis, and highlights the potential impact of this CAMP volcanic phase on the end-Triassic cascade of ecological and biological events.

Previous models on the end-Triassic crisis emphasized diverse aspects of the global-scale climatic and environmental perturbations that led to catastrophic biotic consequences (Beerling and Berner, 2002; Donnadieu et al., 2006; Berner and Beerling, 2007; Bachan and Payne, 2016; Paris et al., 2016; Heimdal et al., 2018, 2020; Landwehrs et al., 2020). Most models focused on the effects of CAMP volcanic emissions (Beerling and Berner, 2002; Donnadieu et al., 2006; Berner and Beerling,

---

2007; Bachan and Payne, 2016; Paris et al., 2016; Landwehrs et al., 2020), but some highlighted the importance of the degassing of sedimentary rocks intruded by CAMP magmas (Heimdal et al., 2018, 2020). Potential positive feedback phenomena were large-scale fires (Belcher et al., 2010) and emissions of methane clathrate (de Wit et al., 2002). Notably, low-δ^{13}C thermogenic gases and clathrates are the optimal carbon sources to reproduce the negative carbon isotope excursions (CIEs) observed in the end-Triassic sedimentary record (Ruhl et al., 2020). Moreover, methane degassing from CAMP intrusive activity (Davies et al., 2017; Capriolo et al., 2021) may explain the deterioration of end-Triassic environmental conditions before the onset of CAMP effusive activity (Larina et al., 2021).

In this study, we considered only the CO_2 from the main volcanic phase of CAMP, which occurred at the beginning of its activity (ca. 201.6–201.5 Ma) and synchronously with the onset of the main extinction phase (Lindström, 2021), in order to assess the potential impact of CAMP volcanism on the end-Triassic climate and environment. Our CO_2 degassing scenarios rely on the content and origin of CO_2 determined through the analysis of melt inclusions within CAMP lava flows (Capriolo et al., 2020) and on the improved geochronological constraints for the early CAMP volcanic activity (Blackburn et al., 2013; Davies et al., 2017; Marzoli et al., 2019). The first CAMP volcanic phase is reasonably well constrained in terms of tempo, volume, eruption style and rate, mainly by geochemical, magnetostratigraphic, biostratigraphic and geochronological data (Knight et al., 2004; Blackburn et al., 2013; Davies et al., 2017; Lindström et al., 2017, 2021; Marzoli et al., 2019; Panfili et al., 2019). This volcanic phase involved brief and intense volcanic pulses, which are individually similar in duration and magnitude of CO_2 degassing to total anthropogenic emissions. Because of their geologically short duration, the climatic and environmental perturbations (generally lasting < 0.01 Ma in our model) triggered by individual volcanic pulses (each lasting ≤ 1000 years in our model; Knight et al., 2004) cannot be detected and temporally resolved in the geological record. However, the similarities between the cumulative model output of the entire first volcanic phase (overall lasting ≤ 0.03 Ma in our model) and the end-Triassic geological record (in terms of atmospheric CO_2 concentration, global average surface temperature, oceanic pH and δ^{13}C) suggest that anthropogenic-scale events may have occurred in Earth's history prior to the Anthropocene.

2. Geological setting

The CAMP covers about 10^7 km^2 of the continents surrounding the Atlantic Ocean (i.e., North America, South America, Africa and Europe), and involves > 3×10^6 km^3 basaltic magmas, emplaced into the continental crust of Pangea at about 201 Ma (Marzoli et al., 1999, 2018). High-quality ^{40}Ar/^{39}Ar dating constrains CAMP magmatic activity to the interval 202–192 Ma, but the peak of magmatism had a duration of < 1 Ma, at the Triassic–Jurassic boundary (Marzoli et al., 2004, 2011, 2018; Nomade et al., 2007). Available U-Pb zircon ages on mostly intrusive CAMP rocks indicates that its peak activity lasted from 201.6 to 200.9 Ma (Fig. 1; Schaltegger et al., 2008; Schoene et al., 2010; Blackburn et al., 2013; Davies et al., 2017, 2021; Heimdal et al., 2018; Marzoli et al., 2019).

The CAMP is constituted of basic rocks erupted as lava flows or intruded at shallow depth within sedimentary basins. Emplacement likely occurred in brief and intense pulses, lasting approximately a few centuries each and characterized by high eruption rates (Knight et al., 2004; Marzoli et al., 2019). The rapidity and magnitude of volcanic eruptions may have been strongly influenced and modulated by volatile species in the transcrustal plumbing system, especially by CO_2 that can act as propellant for magmas during their ascent, triggering pulsed magmatic activity (Black and Manga, 2017; Caricchi et al., 2018; Black and Gibson, 2019; Black et al., 2021). The high volume fraction of CO_2-rich bubbles, entrapped at depth into melt inclusions within CAMP basalts, reveals the abundance of CO_2 in the magmatic plumbing system, suggesting that the entire CAMP emplacement may have degassed up to 10^5 Gt volcanic CO_2 (Capriolo et al., 2020).

The total pre-erosional volume of CAMP can be estimated in 5–6 × 10^6 km^3, considering not only the volume of effusive (minor) and shallow intrusive (major) bodies, but also the volume of the deep transcrustal plumbing system, that was at least partially involved in the degassing process (Capriolo et al., 2020). The effusive CAMP rocks are represented by lava flows, partially preserved by erosion in Triassic–Jurassic sedimentary basins only (~ 0.1 × 10^6 km^3). The shallow intrusive CAMP rocks are represented by sills (> 1.5 × 10^6 km^3), dykes (~ 0.1 × 10^6 km^3; up to 800 km length and up to 300 m width) and layered intrusions (< 0.1 × 10^6 km^3; McHone, 2003; Callegaro et al., 2017; Marzoli et al., 2018). The deep crustal intrusions form the deep plumbing system of CAMP and may be equivalent to about 50–100% of
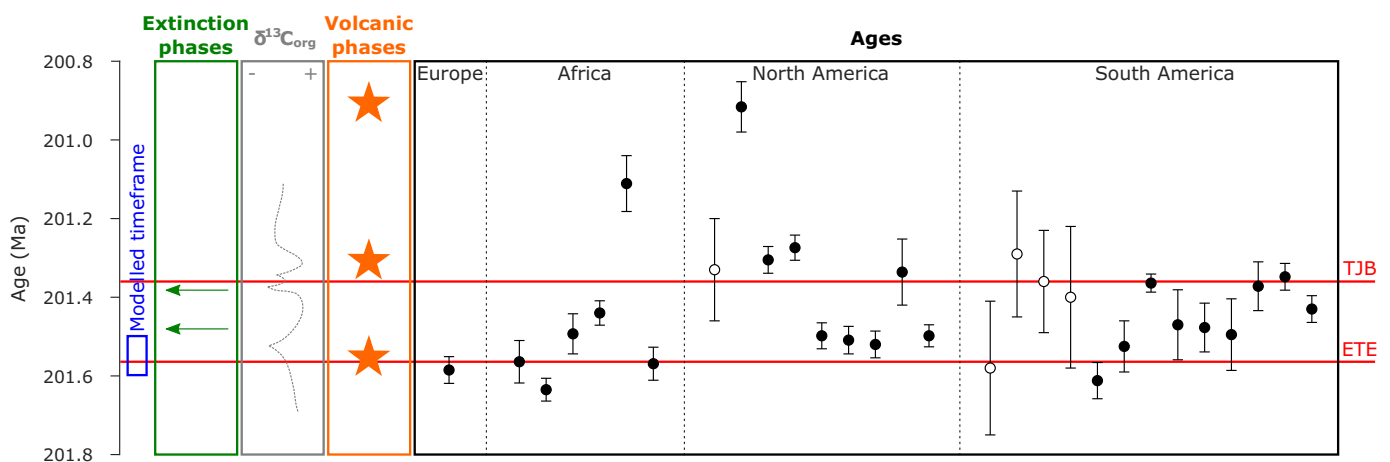
Fig. 1. Plot of the end-Triassic timescale, with the modelled timeframe, the extinction phases, the composite δ^{13}C record of organic matter, the volcanic phases of CAMP activity and the available U-Pb ages for CAMP rocks and volcanic ashes. The Triassic–Jurassic boundary (TJB) is placed at 201.36 ± 0.17 Ma (Wotzlaw et al., 2014), whereas the end-Triassic extinction (ETE) is placed at 201.564 ± 0.015 Ma (Blackburn et al., 2013). The modelled timeframe (201.6–201.5 Ma) is represented by the blue box. The 2 extinction phases are represented by green arrows, after Lindström et al. (2021). The composite δ^{13}C record of organic matter is represented by the grey dotted curve, after Lindström et al. (2017) and references therein. The 3 volcanic phases of CAMP activity (at about 201.6–201.5, 201.3 and 200.9 Ma, respectively) are represented by orange stars. The U-Pb ages of CAMP rocks are represented by filled circles, and those of volcanic ashes are represented by empty circles. The plotted U-Pb ages are from Schaltegger et al. (2008), Schoene et al. (2010), Blackburn et al. (2013), Davies et al. (2017, 2021), Heimdal et al. (2018) and Marzoli et al. (2019). For the interpretation of colours in this figure, the reader is referred to the web version of the article.

the total original volume of effusive and shallow intrusive bodies (Marzoli et al., 2018).

In terms of tempo and emplaced volume, CAMP volcanic activity is best constrained in North America (Blackburn et al., 2013) and Morocco (Marzoli et al., 2019). In particular, combining the time constraints from these CAMP sub-provinces, three main phases of effusive magmatic activity can be identified (Fig. 1; Blackburn et al., 2013; Davies et al., 2017; Marzoli et al., 2019):

- the 1st volcanic phase at about 201.6–201.5 Ma, corresponding to the Talcott Basalt and correlative lava flows (i.e., Orange Mountain Basalt from the Newark basins and North Mountain Basalt from the Fundy basin) in North America (Weems et al., 2016) and to the entire succession from Lower to Upper Basalt in Morocco (Marzoli et al., 2019);
- the 2nd volcanic phase at about 201.3 Ma, corresponding to the Holyoke Basalt and correlative lava flows (i.e., Preakness Basalt from the Newark basins) in North America (Weems et al., 2016) and missing in Morocco;
- the 3rd volcanic phase at about 200.9 Ma, corresponding to the Hampden Basalt and correlative lava flows (i.e., Hook Mountain Basalt from the Newark basins) in North America (Weems et al., 2016) and to the Recurrent Basalt in Morocco (Marzoli et al., 2019).

Lava flows in Portugal and Algeria were mostly emplaced during the 1st volcanic phase, whereas the sills in Amazonia yield ages from 201.525 ± 0.065 to 201.348 ± 0.034 Ma (Davies et al., 2017, 2021; Heimdal et al., 2018), suggesting prolonged intrusive activity lasting from the 1st to the 2nd volcanic phase. These Amazonian sills represent the largest preserved CAMP intrusions at shallow depth ($\sim 1 \times 10^6$ km^3; Marzoli et al., 2018; Capriolo et al., 2021). Hence, most of CAMP effusive activity and also a vast part of CAMP intrusive activity occurred during the 1st volcanic phase (Blackburn et al., 2013; Davies et al., 2017, 2021; Marzoli et al., 2019). In particular, this volcanic phase represents about 55% of the total preserved volcanic rocks in North America, and about 98% of the total preserved volcanic rocks in Morocco (Table 1). This main volcanic phase is subdivided into several short-lived volcanic pulses, as observed in North America and Morocco (Knight et al., 2004; Blackburn et al., 2013; Marzoli et al., 2019). In detail, according to the geochemical, magnetostratigraphic, biostratigraphic and geochronological data in Morocco (Knight et al., 2004; Marzoli et al., 2019; Panfili et al., 2019), the succession from the Lower to the Upper Basalt lava flows was emplaced rapidly, in coincidence with the main phase of the end-Triassic extinction, through 4 short-lived volcanic pulses. Each eruptive pulse likely lasted < 450 years according to magnetostratigraphic constraints (Knight et al., 2004), and was separated from the others by quiescent intervals lasting less than the average analytical error on U-Pb dating (i.e., < 50 ka; ka = thousand years; Marzoli et al., 2019).

3. Materials and methods

In order to investigate the pulsed CO$_2$ degassing of CAMP, we used the biogeochemical box model *CARMER* (Dal Corso et al., 2020) for the carbon cycle only. This model consists of a three-box marine carbon–alkalinity cycle, representing deep ocean, low- and high-latitude surface ocean, linked to a single-box atmosphere and a single-box crust. This model combines aspects from several previous approaches (Walker and Kasting, 1992; Rampino and Caldeira, 2005; Payne and Kump, 2007; Clarkson et al., 2015) and was also used to investigate the Permo–Triassic mass extinction (Dal Corso et al., 2020), as well as the effect of large changes in the Cenozoic calcium cycle (Shields and Mills, 2021). The full details of the model are available in an open access publication (Dal Corso et al., 2020).

We used *CARMER* to assess the potential climatic and environmental impact of the volcanic CO$_2$ emitted during the 1st volcanic phase of CAMP emplacement, which is synchronous with the onset of the end-Triassic mass extinction (Lindström et al., 2017, 2021; Panfili et al., 2019; Lindström, 2021) and corresponds to most of the emplaced magma volume (Table 1). Moreover, this is the only phase of CAMP volcanic activity that can be reasonably well constrained in terms of both tempo and emplaced volume. In comparison, the later CAMP volcanic phases involved less volume, occurred after the main extinction interval, and lack strong constraints especially on the eruption rate. The relatively wide range of ages for CAMP intrusions in Amazonia, spanning about 180 ka (Davies et al., 2017, 2021; Heimdal et al., 2018), hints at prolonged degassing from the intruded organic-rich sediments contrasting with the rapid and pulsed volcanic activity. Several scenarios are tested here, using different degassed volumes, different number or duration of volcanic pulses, different initial conditions, and different isotopic compositions of degassed volcanic CO$_2$ (Table 2).

The age and preserved volumes of the main volcanic phase are precisely characterized and well constrained. The abundance of melt inclusions entrapped at depth within glomerocrystic aggregates of CAMP basalts (Capriolo et al., 2020) suggests that large parts of CAMP magmas reached the CO$_2$ exsolution depth during the emplacement of this LIP in a thinned lithosphere (Tegner et al., 2019). However, we conservatively assumed that only 4×10^6 km^3 of the total CAMP volume (i.e., 5–6 $\times$ 10^6 km^3) was degassed during its emplacement as both lava flows and intrusive bodies, including the shallower portions of the deep plumbing

Table 2
Combination of the parameters considered in the different tested scenarios for the 1st volcanic phase of CAMP.

Degassed CAMP volume	Pulses number	Pulse duration	δ^{13}C of degassed CO$_2$	CO$_2$ baseline
(%)	/	(years)	(‰)	(ppm)
12.5	1	400	−5	820
12.5	1	1000	−5	820
25	4	400	−5	820
50	4	400	−5	820
50	4	400	−5	1180
50	4	400	−20	820
50	10	400	−5	820
50	10	400	−20	820
75	4	400	−5	820

Table 1
Dimensions and proportions estimated for CAMP volcanic formations, corresponding to each volcanic phase, in North America and Morocco.

	Volcanic phases	Thickness (m)	Average thickness (km)	Surface (km^2)	Total volume (km^3)	Volume proportion (%)
North America						
Talcott Basalt	I	130–250	0.19	25,186	4785	55
Holyoke Basalt*	II	200–1200	0.20	14,530	2906	33
Hampden Basalt	III	30–110	0.07	14,530	1017	12
Morocco						
Lower, Intermediate and Upper Basalt	I	100–250	0.12	130,000	15,600	98
Recurrent Basalt	III	5–50	0.03	13,000	390	2

The data for North America are from Weems et al. (2016), and those for Morocco are from Marzoli et al. (2019). The symbol * indicates the presence of sedimentary intercalations within this formation: these sedimentary intercalations are not considered for the estimate of the average thickness and thus of the total volume.

system, following the constrained three main phases of effusive magmatic activity. The 1st volcanic phase of the CAMP corresponds to ~ 55% of the total volume emplaced in North America and ~ 98% of the total volume emplaced in Morocco. Hence, we conservatively assumed that only 50% of the degassed CAMP volume (i.e., 50% of 4×10^6 km^3, corresponding to 2×10^6 km^3) was emplaced during the 1st volcanic phase for the main scenario. Moreover, we assumed an average of 0.5 wt.% CO_2 for all CAMP magmas, since this value is the minimum calculated in the same melt inclusions, displaying moderately differentiated composition and enriched volatile content (Capriolo et al., 2020). Then, considering an average value of 2.90 g/cm^3 for the density of all CAMP basaltic rocks (Moore, 2001), the CAMP volume emplaced during the 1st volcanic phase (i.e., 2×10^6 km^3) may have degassed up to 2.9×10^4 Gt CO_2, for a complete degassing of CO_2 from the magmas.

The total volcanic CO_2 degassed by CAMP magmas during the 1st volcanic phase is modelled as being degassed in equally spaced pulses, starting from 201.6 Ma (i.e., time 0 in our model), each one lasting 400 years. These short-lived volcanic pulses are modelled as square wave-shape spikes, with constant CO_2 flux in time (Fig. 2).

Assuming 50% of the degassed CAMP volume as the most realistic scenario, we modelled 4 pulses, each lasting 0.4 ka and occurring every 10 ka (i.e., stasis of 9.6 ka between each pulse, for a total duration of 30.4 ka). We also modelled 10 pulses, each lasting 0.4 ka and occurring every 3 ka (i.e., stasis of 2.6 ka between each pulse, for a total duration of 27.4 ka), implying a lower annual degassing rate. The 4-pulse model is based on the magnetostratigraphic data in Morocco, where the 1st volcanic pulse corresponds to the base of the Lower Basalt, the 2nd volcanic pulse corresponds to the top of the Lower Basalt, the 3rd volcanic pulse corresponds to the base of the Intermediate Basalt, and the 4th volcanic pulse corresponds to the top of the Intermediate and to the whole Upper Basalt (Knight et al., 2004; Marzoli et al., 2019). The 10-pulse model is arbitrary developed taking into account that the volcanic pulses constrained in Morocco may not be perfectly synchronous with those occurring in other circum-Atlantic basins. Since the total magma volume and thus the total degassed CO_2 are considered the same, each of the 10 volcanic pulses emits 4/10 of CO_2 compared to the 4-pulse model. We assumed the volume associated with each volcanic pulse as equal to 25% of the total volume involved in the 1st volcanic phase for the 4-pulse

model (i.e., 25% of 2×10^6 km^3, corresponding to 5×10^5 km^3), and to 10% of the same total volume for the 10-pulse model (i.e., 10% of 2×10^6 km^3, corresponding to 2×10^5 km^3). Hence, for the 4-pulse model, each volcanic pulse emits a total of 7250 Gt CO_2 (i.e., ca. 1.65×10^{17} mol CO_2) with a degassing rate of 4.12×10^{14} mol/year CO_2 (Fig. 2). Instead, for the 10-pulse model, each volcanic pulse emits a total of 2900 Gt CO_2 (i.e., ca. 6.59×10^{16} mol CO_2) with a degassing rate of 1.65×10^{14} mol/year CO_2 (Fig. 2).

A value of $-5‰$ is assumed for the δ^{13}C of degassed volcanic CO_2, since it is typical of mantle-derived basaltic magmas (Mattey et al., 1984). However, despite having a deep origin, the degassed CO_2 may display different isotopic signatures. This may be derived from mantle heterogeneities, i.e., recycled subducted crustal material (Cartigny et al., 2001; Deines, 2002; Plank and Manning, 2019), or from meta-sedimentary rocks, via assimilation at lower–middle crust during magma rise (Capriolo et al., 2020). In the latter case, the degassed CO_2 could display a δ^{13}C value approximately ranging from $+2‰$ (in the case of a carbonate source) to $-30‰$ (in the case of an organic source), depending on the contribution of each potential source (Schidlowski, 2001). Hence, we also carried out model runs considering $-20‰$ for the δ^{13}C of the degassed volcanic CO_2.

The pre-CAMP atmospheric CO_2 concentration at the end-Triassic is constrained through palaeosol carbonate and stomatal index data (McElwain et al., 1999; Schaller et al., 2011). We conservatively assumed two different initial conditions (i.e., ~ 800 and ~ 1200 ppm), in order to test the differences when assuming values below or above 1000 ppm for the pre-CAMP atmospheric CO_2 concentration.

4. Results

The main scenario for modelling the 1st volcanic phase of CAMP activity, starting from 201.6 Ma, is based on the assumptions that it involves about 50% of the degassed CAMP volume, as observed in North America, and it displays 4 pulses, which are well constrained in Morocco. However, in order to test other potential scenarios, we modelled also the possibility that respectively 25% and 75% of the CAMP volume was emplaced, thus degassed during the 1st volcanic phase (Fig. 3).

Starting from a value of ~ 800 ppm for the pre-CAMP baseline, the maximum concentration of atmospheric CO_2 (i.e., at the peak of the last, fourth volcanic pulse) reaches ca. 1250 ppm for the first scenario (emplacement of 25 vol.% of the total CAMP magmas during the 1st volcanic phase), ca. 1750 ppm for the second scenario (emplacement of 50 vol.% of the total CAMP magmas during the 1st volcanic phase), and ca. 2250 ppm for the third scenario (emplacement of 75 vol.% of the total CAMP magmas during the 1st volcanic phase). These values correspond to an increase of the global average surface temperature respectively of about 3, 5 and 7 °C, from the initial value of ~ 23 °C, and to a decrease of the oceanic pH at low latitudes respectively of about 0.1, 0.2 and 0.3 log units, from the initial value of ~ 8.1 log units. In all the proposed scenarios, the negative shift of the oceanic δ^{13}C at low latitudes is $< 1‰$, from the initial value of ~ 0.7‰.

The main model (i.e., 50% of the degassed CAMP volume and 4 pulses) is tested using two different initial conditions for the end-Triassic atmospheric CO_2 concentration (i.e., ~ 800 and ~ 1200 ppm; Fig. 4a and b). The main difference between these two models is the maximum atmospheric CO_2 concentration achieved after the injection of CAMP volcanic CO_2, which reflects the gap between the initial conditions. In detail, the model using ~ 800 ppm as a baseline reaches ca. 1750 ppm CO_2, and the model using ~ 1200 ppm as a baseline reaches ca. 2150 ppm CO_2. Therefore, even if the maximum increase in atmospheric CO_2 concentration is the same in both models (i.e., about 950 ppm), the model starting from a lower initial CO_2 concentration (thus, lower initial temperature) displays an increase in the global average surface temperature of 5 °C, while the model starting from a higher initial CO_2 concentration (thus, higher initial temperature) displays an increase in
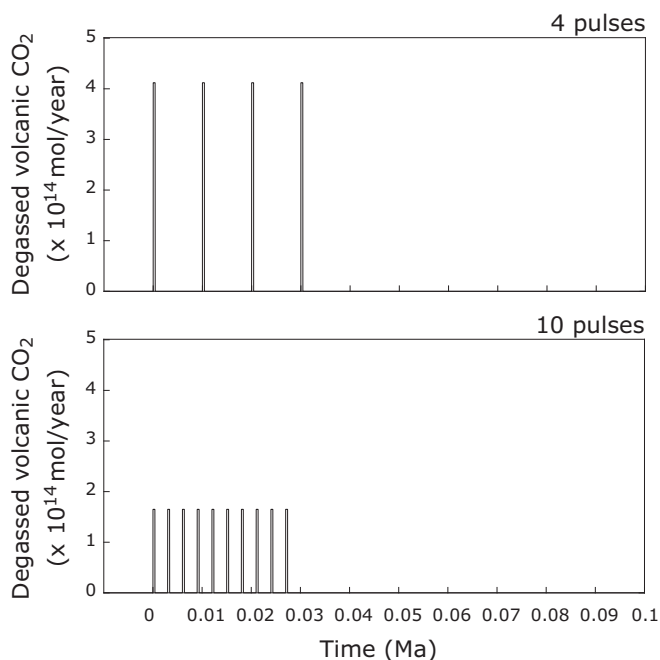
Fig. 2. Comparison between annual fluxes of 4- and 10-pulse models for the first phase of CAMP volcanic activity.
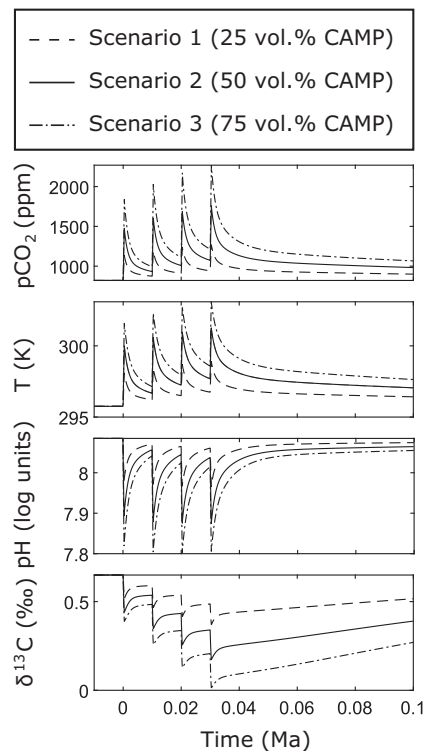
Fig. 3. Potential scenarios for the 1st volcanic phase of CAMP activity. Comparison between the different modelled scenarios, involving different amounts of degassed magma: 25%, 50% and 75% of the degassed CAMP volume. The volcanic CO_2 degassing rate is 2.06×10^{14} mol/year for scenario 1, 4.12×10^{14} mol/year for scenario 2 and 6.18×10^{14} mol/year for scenario 3. Plots of several output proxies (atmospheric CO_2 concentration, global average surface temperature, oceanic pH at low latitudes and oceanic $\delta^{13}C$ at low latitudes) versus time, where model time 0 corresponds to 201.6 Ma.

the global average surface temperature of 4 °C. A similar difference is also observed in the ocean temperatures. However, the differences in the variation of both pH and $\delta^{13}C$ between these two models are negligible.

The alternative model, implying 10 pulses for the same degassed volume, is tested using the initial condition of ~ 800 ppm for the end-Triassic atmospheric CO_2 concentration (Fig. 4c). This scenario dilutes the same total amount of CO_2 emitted in the 4-pulse model into 10 volcanic pulses, with same duration and shorter spacing, during a similar interval of time. Hence, all the proxy variations of this model are dampened compared to the 4-pulse model. For instance, the maximum concentration of atmospheric CO_2 (i.e., at the peak of the last, tenth volcanic pulse) reaches ca. 1500 ppm, from the initial value of ~ 800 ppm, and the global average surface temperature reaches ca. 27 °C, from the initial value of ~ 23 °C. This difference is due to the negative feedbacks of the system, including the transport of CO_2 into the ocean, its accumulation in the deep ocean and its burial in sediments. Larger individual volcanic pulses would be more capable of overwhelming these feedbacks and causing a rise of atmospheric CO_2.

Furthermore, we tested both the main and alternative models (i.e., respectively with 4 and 10 pulses) using a $\delta^{13}C$ value of −20‰ instead of the typical $\delta^{13}C$ value of −5‰ for the degassed CO_2 (Fig. 5a and b). Compared to the −5‰ $\delta^{13}C$ scenarios, the −20‰ $\delta^{13}C$ scenarios result in a negative shift of about 6‰ for atmospheric $\delta^{13}C$ in both 4- and 10-pulse models. Moreover, these scenarios indicate also a negative shift of about 1.5‰ for oceanic $\delta^{13}C$ in both 4- and 10-pulse models.

In order to evaluate the impact of a single CAMP volcanic pulse and especially of its degassing rate on climatic and environmental changes, we modelled two different single pulse scenarios, using the same degassed volume (i.e., the same amount emitted from each pulse in the

main, 4-pulse model) and different duration, respectively 400 and 1000 years (Fig. 6a and b). This comparison highlights that for the same amount of emitted CO_2 the event with shorter duration leads to slightly more extreme variations compared to the event with longer duration for most output proxies.

The same *CARMER* model is also applied to total anthropogenic emissions of CO_2 (Fig. 6c), in order to compare them with a single CAMP volcanic pulse. We used the data of global CO_2 emissions via fossil fuel burning, cement production and gas flaring from the Industrial Revolution (i.e., 1751 C.E.) to the present days (i.e., 2014 C.E.; Boden et al., 2017). Furthermore, the comparison between the results of Anthropocene model and the modern record for different climate variables, based on both direct measurements and proxy data (Supplementary Fig. 1), confirms the reliability of this biogeochemical box model, used also for CAMP degassing activity.

5. Discussion

Although the main constraints for CAMP volcanic phases hinge on the same geographical areas where CAMP volcanic formations are best preserved (i.e., North America and Morocco), the here proposed scenarios substantially differ from those of the previous studies (Beerling and Berner, 2002; Donnadieu et al., 2006; Berner and Beerling, 2007; Bachan and Payne, 2016; Paris et al., 2016; Heimdal et al., 2018, 2020; Landwehrs et al., 2020). Most of the previous studies have modelled potential emission pulses for all the CAMP volcanic phases, whereas we detailed potential emission pulses on a higher-resolution timescale and exclusively for the first CAMP volcanic phase, since this is volumetrically dominant and coincides with the main extinction interval (Lindström, 2021). This phase is here modelled as 4 to 10 short-lived ($\leq$ 1000 years) volcanic pulses in a 0.1 Ma timeframe ($\leq$ 0.03 Ma for the total degassing). The volcanic CO_2 emissions are constrained by recently published melt inclusion data (Capriolo et al., 2020), used for the first time in modelling CAMP activity.

The results of our biogeochemical box model indicate climate instability and environmental variability on a 100–1000 years timeframe, induced by the rapid and pulsed degassing activity of CAMP. This period of extreme climatic and environmental instability coincided in time with the end-Triassic biosphere crisis and likely drove it via stressors, such as extreme warming, ocean acidification and hypoxia (Kiessling and Aberhan, 2007; Deenen et al., 2010; Pálfy and Zajzon, 2012; Kocsis et al., 2014; van de Schootbrugge and Wignall, 2016; He et al., 2020; Wignall and Atkinson, 2020; Hautmann, 2021). This process is reflected by strong extinction selectivity in the marine and terrestrial realms (McRoberts and Newton, 1995; Dunhill and Wills, 2015; Dunhill et al., 2018b; Allen et al., 2019), casting doubt on the hypothesis of a crisis resulted from a gradual increase in extinction rates throughout the Late Triassic (Hallam, 2002; Tanner et al., 2004; Lucas and Tanner, 2018). The devastating impact of CAMP volcanism on the end-Triassic biota is also supported by the high occurrence of abnormal fern spores, revealing plant mutagenesis that is likely related to volcanic mercury (Lindström et al., 2019).

The carbon cycle perturbations reconstructed from the end-Triassic stratigraphic record imply atmospheric CO_2 variations, a carbonate productivity crisis and negative CIEs (Paris et al., 2016). The pedogenic carbonate and stomatal index proxies suggest an increase of both atmospheric CO_2 and global average surface temperature at the Triassic–Jurassic boundary (McElwain et al., 1999; Schaller et al., 2011). Palaeosol carbonates indicate that atmospheric CO_2 increased from 2000 to 4400 ppm, and each CAMP volcanic pulse caused an increase about 2000 ppm of atmospheric CO_2 (Schaller et al., 2011). Stomatal indices suggest that atmospheric CO_2 increased from 600 to 2100–2400 ppm, implying a global average surface temperature increase of 3–4 °C (McElwain et al., 1999). The data based on stomatal indices (McElwain et al., 1999) are consistent with the results of our modelling, corresponding to the atmospheric CO_2 values expected immediately after
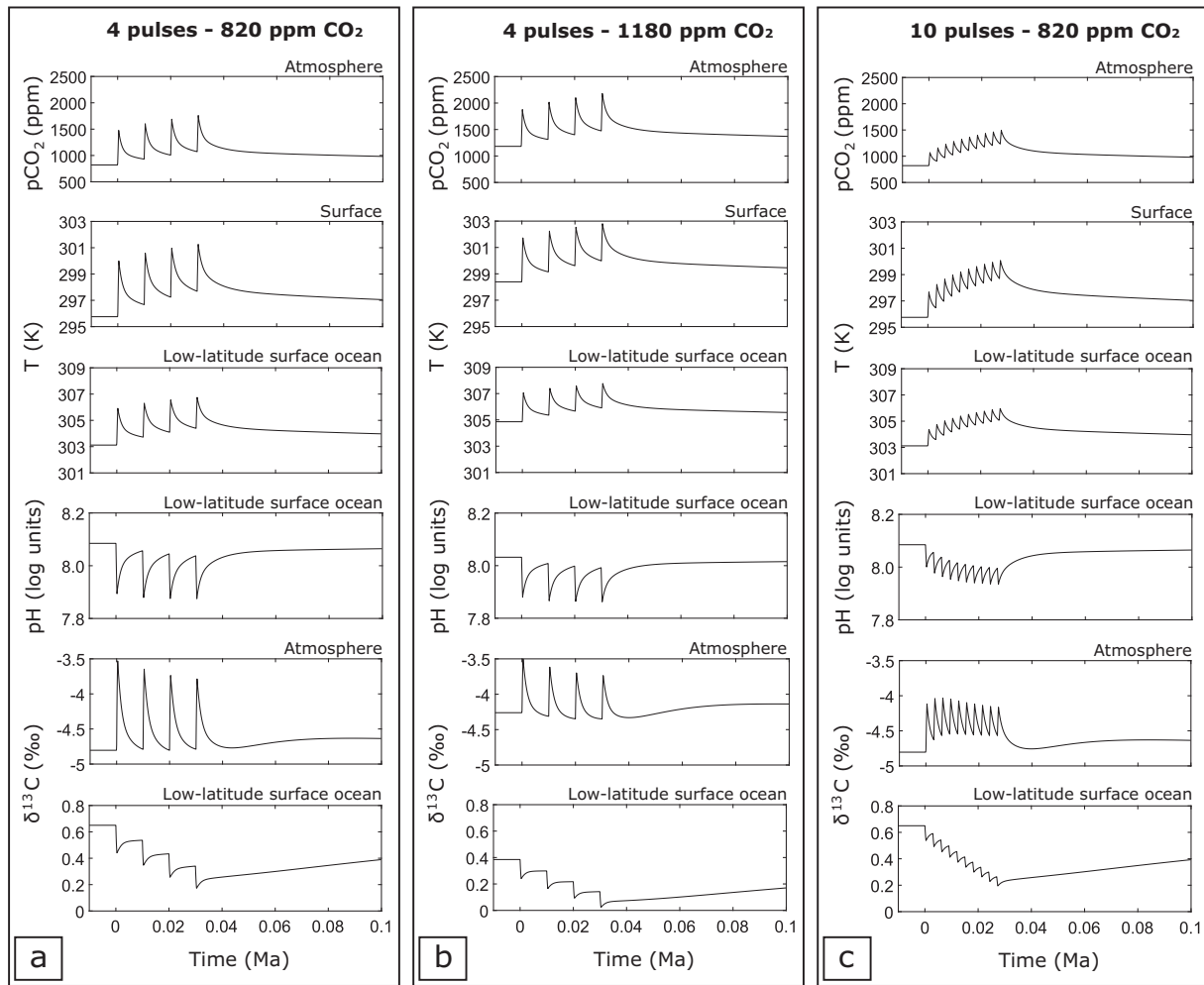
Fig. 4. Output proxies for the main and alternative models. The output proxies are atmospheric CO_2 concentration, temperature, oceanic pH and $\delta^{13}C$. These models involve 50% of the degassed CAMP volume, $-5‰$ isotopic signature for the degassed carbon and ~ 800 or ~ 1200 ppm CO_2 concentration for the end-Triassic atmosphere. a) 4-pulse model with CO_2 baseline at ~ 800 ppm, the degassing rate is 4.12×10^{14} mol/year. b) 4-pulse model with CO_2 baseline at ~ 1200 ppm, the degassing rate is 4.12×10^{14} mol/year. c) 10-pulse model with CO_2 baseline at ~ 800 ppm, the degassing rate is 1.65×10^{14} mol/year.
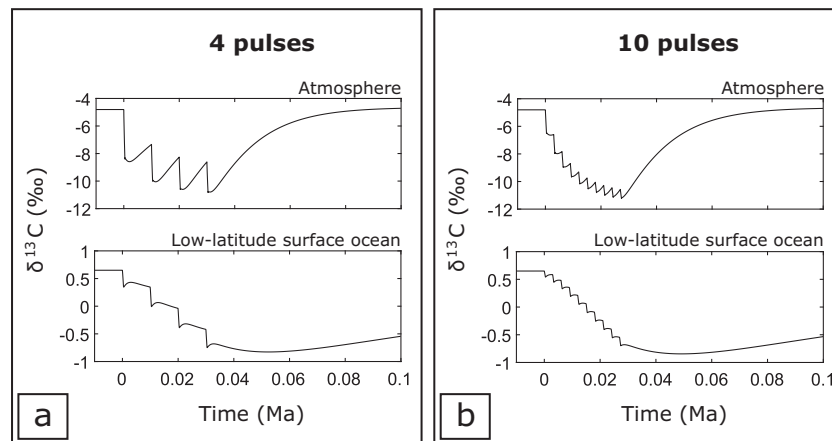
Fig. 5. Output $\delta^{13}C$ for both 4- and 10-pulse models with more negative isotopic signature. These models involve 50% of the degassed CAMP volume, $-20‰$ isotopic signature for the degassed carbon and ~ 800 ppm CO_2 concentration for the end-Triassic atmosphere. a) Plots of atmospheric and oceanic $\delta^{13}C$ for the 4-pulse model, the degassing rate is 4.12×10^{14} mol/year. b) Plots of atmospheric and oceanic $\delta^{13}C$ for the 10-pulse model, the degassing rate is 1.65×10^{14} mol/year.

Fig. 6. Output proxies for different single CAMP pulse scenarios, with same degassed volume and different duration, and for the anthropogenic emissions. The output proxies are atmospheric CO_2 concentration, temperature, oceanic pH and $\delta^{13}C$. For single CAMP pulse scena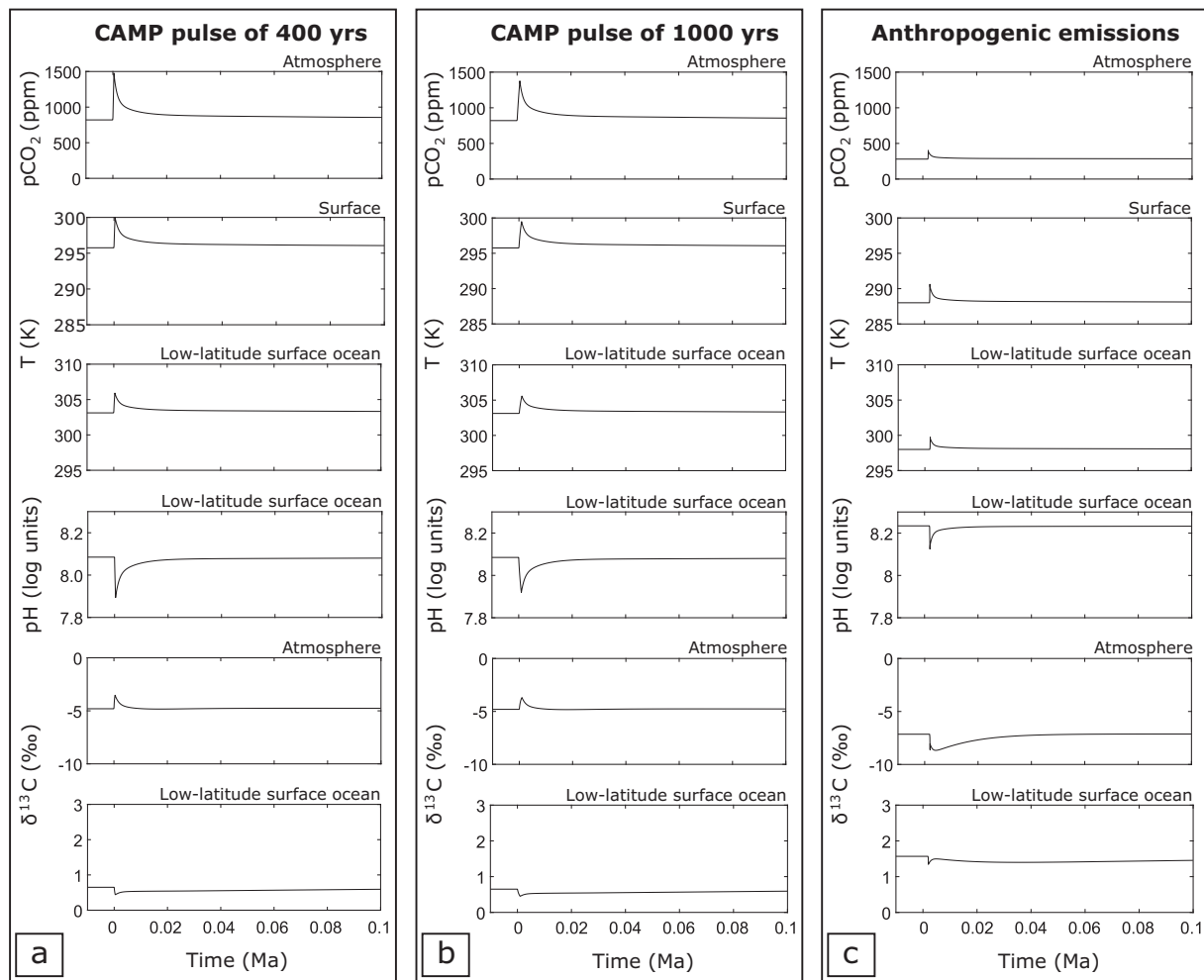rios, the degassed volume is 1.65×10^{17} mol CO_2, the same as for each pulse in the main model (i.e., 50% of the degassed CAMP volume and 4 pulses). a) Plots of output proxies versus time for the 400 years-lasting pulse scenario, the degassing rate is 4.12×10^{14} mol/year. b) Plots of output proxies versus time for the 1000 years-lasting pulse scenario, the degassing rate is 1.65×10^{14} mol/year. c) Plots of output proxies versus time for CO_2 anthropogenic emissions, where model time 0 corresponds to 1 B.C.E. and the $\delta^{13}C$ of CO_2 input is −23‰.

CAMP volcanic activity. However, starting from higher initial values of atmospheric CO_2, the data based on palaeosol carbonates (Schaller et al., 2011) indicate also higher values of atmospheric CO_2 after CAMP volcanic activity, that may have occurred only for a very short period, post-eruption and pre-recovery. After each major volcanic pulse, the atmospheric CO_2 levels declined because of the silicate weathering of freshly erupted lavas (Schaller et al., 2011).

A general short-term ocean acidification, mainly affecting the benthic communities, likely triggered a long-term biotic crisis (Hautmann, 2004; Kiessling and Simpson, 2011; Greene et al., 2012; Hönisch et al., 2012; Martindale et al., 2012; Fujisaki et al., 2018). The occurrence of ocean acidification during the end-Triassic extinction interval is testified by a decline of carbonate productivity (Clémence et al., 2010; Greene et al., 2012). However, the effects of lower seawater pH vary considerably among stratigraphic sections depending on the local variations of carbonate palaeoenvironments (Todaro et al., 2018). The rapid and pulsed input of volcanic CO_2 into the surface system may thus have caused significant global warming and ocean acidification, both of which are possible kill mechanisms for the end-Triassic mass extinction (Wignall, 2015; Dunhill et al., 2018b).

The end-Triassic CIEs reflect a major perturbation of the global carbon cycle, consistent with an injection of isotopically light carbon into the surface system (Hesselbo et al., 2002). Only the results deriving

from −20‰ as $\delta^{13}C$ of CO_2 input may fit with the $\delta^{13}C$ record of carbonates, considering the precursor CIE, known as *Marshi*, in coincidence with the beginning of CAMP magmatism at the end-Triassic (Lindström et al., 2017, 2021; Panfili et al., 2019; Lindström, 2021). Despite the slight differences in the magnitude of the negative CIE shifts from different geographical areas (Greene et al., 2012), the larger negative CIE shift (about 1.5‰) produced using −20‰ as $\delta^{13}C$ of CO_2 input is mostly consistent with the first end-Triassic $\delta^{13}C$ shift of marine carbonates (generally < 3.0‰; Pálfy et al., 2001, 2007; Korte et al., 2009; Clémence et al., 2010; Bachan et al., 2012; Todaro et al., 2018), lasting less than 0.1 Ma (Yager et al., 2017). This suggests that the isotopic composition of volcanic CO_2 may be more negative than the typically assumed $\delta^{13}C$ value of −5‰ (Mattey et al., 1984), or that other potential carbon sources may have been involved during CAMP emplacement (Heimdal et al., 2020; Capriolo et al., 2021).

This study considers only the volcanic component of CO_2, since this is the only volatile species quantitatively constrained via the investigation of melt inclusions (Capriolo et al., 2020). As CO_2 exsolution started from lower–middle crustal depths (Capriolo et al., 2020), most of the intrusive CAMP magmas likely contributed to the volcanic CO_2 emissions. However, other volcanic volatile species may play a key role in the climatic and environmental perturbations. Sulphur species (e.g., SO_2 and H_2S) may have impacted climate, environment and biota (Wignall,

2001; Callegaro et al., 2014). In the atmosphere, volcanic SO_2 may react with H_2O to cause acid rains and form aerosols, responsible for an increase of the atmospheric optical depth with subsequent global cooling (Black et al., 2012, 2014, 2021). Stratigraphic, biostratigraphic and isotopic data support the occurrence of a repeated release of SO_2-dominated volatiles before the main accumulation of CO_2-dominated volatiles from CAMP degassing (Guex et al., 2004, 2016; Schoene et al., 2010). Previous studies on the activity of LIPs modelled the dynamic response of Earth system to the volcanic outgassing of both carbon and sulphur (e.g., Black et al., 2018; Landwehrs et al., 2020), suggesting that the combined emission of these volatile species may lead to a systemic global-scale swing in temperature, with a shorter-term cooling phase followed by a longer-term warming phase. However, global cooling events due to volcanic emissions of sulphur species have a geologically very short duration, in the order of a few years (Schmidt et al., 2016; Landwehrs et al., 2020).

Although at a higher-resolution timescale (≤ 1000 years) compared to previous models on CAMP activity (Berner and Beerling, 2007; Bachan and Payne, 2016; Paris et al., 2016; Landwehrs et al., 2020), our model results highlight the importance of CO_2 release in short-lived pulses to reproduce the climatic and environmental disruption reconstructed from the end-Triassic geological record. Moreover, brief volcanic pulses mean less variation in the $\delta^{13}C$ record for the same increase of global average surface temperature, implying that major climatic and environmental changes could be hidden in deep-time geological record. Our modelled scenarios also show the rough similarity between each CAMP volcanic pulse at the end-Triassic (in the 4-pulse model) and total anthropogenic emissions, in terms of both intensity and duration of the CO_2 fluxes. In detail, each pulse of the first volcanic phase of CAMP released about 1.7×10^{17} mol CO_2 in about 400 years, and the total anthropogenic emissions released about 3.4×10^{16} mol CO_2 in about 250 years. The degassing rate of each CAMP volcanic pulse is thus about 4.1×10^{14} mol/year CO_2, which is interestingly comparable to the current values of anthropogenic emissions (about 8.2×10^{14} mol/year CO_2 at 2014 C.E.; Boden et al., 2017).

6. Conclusions

Our biogeochemical model is constrained by melt inclusion data on CO_2 source and concentration in CAMP basaltic magmas along with stratigraphic, magnetostratigraphic, biostratigraphic, geochronological and geochemical data on CAMP lava flows. This model focuses on the volcanic CO_2 degassing from the main volcanic phase of CAMP emplacement (ca. 201.6–201.5 Ma), and shows the key role of this LIP in the rapid global-scale climatic and environmental changes that triggered the end-Triassic mass extinction. The degassing activity of CAMP, through rapid and pulsed injections of volcanic CO_2 into the end-Triassic surface system, may indeed have disrupted the climatic and environmental equilibria, triggering a cascade of catastrophic ecological and biological consequences. The impact of CAMP volcanic activity may likely have been enhanced by thermogenic degassing (i.e., from organic-, carbonate- or evaporite-rich materials intruded by CAMP) and positive feedback phenomena (i.e., large-scale fires and methane clathrate destabilization). Our model results are generally consistent with some recent palaeoclimatic models on the end-Triassic, which consider alternatively intrusive or effusive activity of CAMP (Paris et al., 2016; Heimdal et al., 2018, 2020; Landwehrs et al., 2020). However, unlike the models of CAMP intrusive activity (Heimdal et al., 2018, 2020), here we demonstrated that CAMP volcanic volatiles, through very short-lived pulses, are sufficient to trigger global-scale climatic and environmental disruption, playing a fundamental role in the end-Triassic biotic crisis.

Brief, episodic and intense natural events from Earth's history, such as individual LIP pulses, may cause effects on the global-scale climate and environment comparable to those of current anthropogenic emissions. Nevertheless, anthropogenic-scale events from Earth's past can be hidden in the geological record because of their short duration and the lack of a continuous sedimentary record with high resolution. According to our model results, the intensity of climatic, environmental, thus ecological and biological changes depends on the number, duration and intensity of the eruptive pulses, as well as on the interval between them. However, regardless of how many volcanic pulses, how long and which isotopic signature for the degassed CO_2 are assumed, our modelling shows that volcanic activity alone can substantially increase the atmospheric CO_2 and thus the global average surface temperature, and can decrease the oceanic pH (i.e., ocean acidification). This study highlights the importance of short and intense episodes of CO_2 degassing in driving the extreme rates of climatic and environmental changes, via the injection of huge amounts of volcanic CO_2 into the atmosphere–hydrosphere system, and the consequent oceanic pH drop. Evidence that mass extinction events may be associated with anthropogenic-scale CO_2 inputs on the 100s years timeframe is of obvious concern given current levels of CO_2 emissions, and opens new possibilities for the interpretation of the climatic and environmental impact of LIP activity.

Data and code availability

The datasets used in this manuscript are from already published literature, as cited in the text, and the MATLAB code for *CARMER* model is available from B.J.W.M. on request.

Author contributions

B.J.W.M., R.J.N., J.D.C. and A.M. devised the project. M.C. designed the model scenarios with fundamental inputs from B.J.W.M., R.J.N., J.D.C. and A.M. All authors contributed to the multidisciplinary aspects and writing of the manuscript.

Declaration of Competing Interest

Authors declare no competing interests.

Appendix A. Supplementary data

Supplementary data to this article can be found online at https://doi.org/10.1016/j.gloplacha.2021.103731.

References

Allen, B.J., Stubbs, T.L., Benton, M.J., Puttick, M.N., 2019. Archosauromorph extinction selectivity during the Triassic-Jurassic mass extinction. Palaeontology 62 (2), 211–224.

Alroy, J., 2010. The shifting balance of diversity among major marine animal groups. Science 329, 1191–1194.

Bachan, A., Payne, J.L., 2016. Modelling the impact of pulsed CAMP volcanism on pCO_2 and $\delta^{13}C$ across the Triassic-Jurassic transition. Geol. Mag. 153 (2), 252–270.

Bachan, A., et al., 2012. Carbon cycle dynamics following the end-Triassic mass extinction: constraints from paired $\delta^{13}C_{carb}$ and $\delta^{13}C_{org}$ records. Geochem. Geophys. Geosyst. 13, Q09008.

Beerling, D.J., Berner, R.A., 2002. Biogeochemical constraints on the Triassic-Jurassic boundary carbon cycle event. Glob. Biogeochem. Cycles 16 (3), 1036.

Belcher, C.M., et al., 2010. Increased fire activity at the Triassic/Jurassic boundary in Greenland due to climate-driven floral change. Nat. Geosci. 3, 426–429.

Berner, R.A., Beerling, D.J., 2007. Volcanic degassing necessary to produce a CaCO$_3$ undersaturated ocean at the Triassic–Jurassic boundary. Palaeogeogr. Palaeoclimatol. Palaeoecol. 244, 368–373.

Black, B.A., Gibson, S.A., 2019. Deep carbon and the life cycle of Large Igneous Provinces. Elements 15, 319–324.

Black, B.A., Manga, M., 2017. Volatiles and the tempo of flood basalt magmatism. Earth Planet. Sci. Lett. 458, 130–140.

Black, B.A., Elkins-Tanton, L.T., Rowe, M.C., Peate, I.U., 2012. Magnitude and consequences of volatile release from the Siberian Traps. Earth Planet. Sci. Lett. 317-318, 363–373.

Black, B.A., Lamarque, J.-F., Shields, C.A., Elkins-Tanton, L.T., Kiehl, J.T., 2014. Acid rain and ozone depletion from pulsed Siberian Traps magmatism. Geology 42, 67–70.

Black, B.A., et al., 2018. Systemic swings in end-Permian climate from Siberian Traps carbon and sulfur outgassing. Nat. Geosci. 11, 949–954.

Black, B.A., Karlstrom, L., Mather, T.A., 2021. The life cycle of Large Igneous Provinces. Nat. Rev. Earth Environ. 2, 840–857.

Blackburn, T.J., et al., 2013. Zircon U-Pb geochronology links the end-Triassic extinction with the Central Atlantic magmatic province. Science 340, 941–945.

Boden, T.A., Marland, G., Andres, R.J., 2017. Global, Regional, and National Fossil-Fuel CO$_2$ Emissions. Carbon Dioxide Information Analysis Center, Oak Ridge National Laboratory, U.S. Department of Energy, Oak Ridge, Tennessee, U.S.A. https://doi.org/10.3334/CDIAC/00001_V2017.

Bond, D.P.G., Grasby, S.E., 2017. On the causes of mass extinctions. Palaeogeogr. Palaeoclimatol. Palaeoecol. 478, 3–29.

Callegaro, S., et al., 2014. Microanalyses link sulfur from large igneous provinces and Mesozoic mass extinctions. Geology 42, 895–898.

Callegaro, S., et al., 2017. Geochemical constraints provided by the Freetown layered complex (Sierra Leone) on the origin of high-Ti tholeiitic CAMP magmas. J. Petrol. 58, 1811–1840.

Capriolo, M., et al., 2020. Deep CO$_2$ in the end-Triassic Central Atlantic Magmatic Province. Nat. Commun. 11, 1670.

Capriolo, M., et al., 2021. Massive methane fluxing from magma–sediment interaction in the end-Triassic Central Atlantic Magmatic Province. Nat. Commun. 12, 5534.

Caricchi, L., Sheldrake, T.E., Blundy, J., 2018. Modulation of magmatic processes by CO$_2$ flushing. Earth Planet. Sci. Lett. 491, 160–171.

Cartigny, P., Jendrzejewski, N., Pineau, F., Petit, E., Javoy, M., 2001. Volatile (C, N, Ar) variability in MORB and the respective roles of mantle source heterogeneity and degassing: the case of the Southwest Indian Ridge. Earth Planet. Sci. Lett. 194, 241–257.

Clarkson, M.O., et al., 2015. Ocean acidification and the Permo-Triassic mass extinction. Science 348, 229–232.

Clémence, M.-E., et al., 2010. Bentho-planktonic evidence from the Austrian Alps for a decline in sea-surface carbonate production at the end of the Triassic. Swiss J. Geosci. 103, 293–315.

Courtillot, V.E., Renne, P.R., 2003. On the ages of flood basalt events. Compt. Rendus Geosci. 335, 113–140.

Dal Corso, J., et al., 2020. Permo-Triassic boundary carbon and mercury cycling linked to terrestrial ecosystem collapse. Nat. Commun. 11, 2962.

Davies, J.H.F.L., et al., 2017. End-Triassic mass extinction started by intrusive CAMP activity. Nat. Commun. 8, 15596.

Davies, J.H.F.L., et al., 2021. Zircon petrochronology in large igneous provinces reveals upper crustal contamination processes: new U-Pb ages, Hf and O isotopes, and trace elements from the Central Atlantic magmatic province (CAMP). Contrib. Mineral. Petrol. 176, 9.

de Wit, M.J., et al., 2002. Multiple organic carbon isotope reversals across the Permo-Triassic boundary of terrestrial Gondwana sequences: clues to extinction patterns and delayed ecosystem recovery. J. Geol. 110, 227–240.

Deenen, M.H.L., et al., 2010. A new chronology for the end-Triassic mass extinction. Earth Planet. Sci. Lett. 291, 113–125.

Deines, P., 2002. The carbon isotope geochemistry of mantle xenoliths. Earth-Sci. Rev. 58, 247–278.

Donnadieu, Y., et al., 2006. A GEOCLIM simulation of climatic and biogeochemical consequences of Pangea breakup. Geochem. Geophys. Geosyst. 7, Q11019.

Dunhill, A., Wills, M., 2015. Geographic range did not confer resilience to extinction in terrestrial vertebrates at the end-Triassic crisis. Nat. Commun. 6, 7980.

Dunhill, A.M., Foster, W.J., Sciberras, J., Twitchett, R.J., 2018a. Impact of the Late Triassic mass extinction on functional diversity and composition of marine ecosystems. Palaeontology 61 (1), 133–148.

Dunhill, A.M., Foster, W.J., Azaele, S., Sciberras, J., Twitchett, R.J., 2018b. Modelling determinants of extinction across two Mesozoic hyperthermal events. Proc. R. Soc. B 285, 20180404.

Fujisaki, W., et al., 2018. Global perturbations of carbon cycle during the Triassic–Jurassic transition recorded in the mid-Panthalassa. Earth Planet. Sci. Lett. 500, 105–116.

Greene, S.E., et al., 2012. Recognising ocean acidification in deep time: an evaluation of the evidence for acidification across the Triassic-Jurassic boundary. Earth-Sci. Rev. 113, 72–93.

Guex, J., Bartolini, A., Atudorei, V., Taylor, D., 2004. High-resolution ammonite and carbon isotope stratigraphy across the Triassic–Jurassic boundary at New York Canyon (Nevada). Earth Planet. Sci. Lett. 225, 29–41.

Guex, J., et al., 2016. Thermal erosion of cratonic lithosphere as a potential trigger for mass-extinction. Sci. Rep. 6, 23168.

Hallam, A., 2002. How catastrophic was the end-Triassic mass extinction? Lethaia 35, 147–157.

Hallam, A., Wignall, P.B., 1999. Mass extinctions and sea-level changes. Earth-Sci. Rev. 48, 217–250.

Hautmann, M., 2004. Effect of end-Triassic CO$_2$ maximum on carbonate sedimentation and marine mass extinction. Facies 50, 257–261.

Hautmann, M., 2021. Extinction: end-Triassic mass extinction. eLS 2, 1–15.

He, T., et al., 2020. An enormous sulfur isotope excursion indicates marine anoxia during the end-Triassic mass extinction. Sci. Adv. 6, eabb6704.

Heimdal, T.H., Svensen, H.H., Ramezani, J., et al., 2018. Large-scale sill emplacement in Brazil as a trigger for the end-Triassic crisis. Sci. Rep. 8, 141.

Heimdal, T.H., Jones, M.T., Svensen, H.H., 2020. Thermogenic carbon release from the Central Atlantic magmatic province caused major end-Triassic carbon cycle perturbations. Proc. Natl. Acad. Sci. U. S. A. 117 (22), 11968–11974.

Hesselbo, S.P., Robinson, S.A., Surlyk, F., Piasecki, S., 2002. Terrestrial and marine extinction at the Triassic-Jurassic boundary synchronized with major carbon-cycle perturbation: a link to initiation of massive volcanism? Geology 30, 251–254.

Hönisch, B., et al., 2012. The geological record of ocean acidification. Science 335, 1058–1063.

Kiessling, W., Aberhan, M., 2007. Environmental determinants of marine benthic biodiversity dynamics through Triassic-Jurassic time. Paleobiology 33 (3), 414–434.

Kiessling, W., Simpson, C., 2011. On the potential for ocean acidification to be a general cause of ancient crises. Glob. Chang. Biol. 17, 56–67.

Knight, K.B., et al., 2004. The Central Atlantic Magmatic Province at the Triassic-Jurassic boundary: paleomagnetic and ^{40}Ar/^{39}Ar evidence from Morocco for brief, episodic volcanism. Earth Planet. Sci. Lett. 228, 143–160.

Kocsis, Á.T., Kiessling, W., Pálfy, J., 2014. Radiolarian biodiversity dynamics through the Triassic and Jurassic: implications for proximate causes of the end-Triassic mass extinction. Paleobiology 40 (4), 625–639.

Korte, C., Hesselbo, S.P., Jenkyns, H.C., Rickaby, R.E.M., Spötl, C., 2009. Palaeoenvironmental significance of carbon- and oxygen-isotope stratigraphy of marine Triassic–Jurassic boundary sections in SW Britain. J. Geol. Soc. Lond. 166, 431–445.

Landwehrs, J.P., Feulner, G., Hofmann, M., Petri, S., 2020. Climatic fluctuations modeled for carbon and sulfur emissions from end-Triassic volcanism. Earth Planet. Sci. Lett. 537, 116174.

Larina, E., et al., 2021. Ecosystem change and carbon cycle perturbation preceded the end-Triassic mass extinction. Earth Planet. Sci. Lett. 576, 117180.

Lindström, S., 2021. Two-phased mass rarity and extinction in land plants during the end-Triassic climate crisis. Front. Earth Sci. 9, 780343.

Lindström, S., et al., 2017. A new correlation of Triassic-Jurassic boundary successions in NW Europe, Nevada and Peru, and the Central Atlantic Magmatic Province: a time-line for the end-Triassic mass extinction. Palaeogeogr. Palaeoclimatol. Palaeoecol. 478, 80–102.

Lindström, S., et al., 2019. Volcanic mercury and mutagenesis in land plants during the end-Triassic mass extinction. Sci. Adv. 5, eaaw4018.

Lindström, S., et al., 2021. Tracing volcanic emissions from the Central Atlantic Magmatic Province in the sedimentary record. Earth-Sci. Rev. 212, 103444.

Lucas, S.G., Tanner, L.H., 2018. The missing mass extinction at the Triassic-Jurassic boundary. Chapter 15 In The Late Triassic World. Top. Geobiol. 46, 721–785.

Martindale, R.C., Berelson, W.M., Corsetti, F.A., Bottjer, D.J., West, A.J., 2012. Constraining carbonate chemistry at a potential ocean acidification event (the Triassic-Jurassic boundary) using the presence of corals and coral reefs in the fossil record. Palaeogeogr. Palaeoclimatol. Palaeoecol. 350-352, 114–123.

Marzoli, A., et al., 1999. Extensive 200-million-year-old continental flood basalts of the Central Atlantic Magmatic Province. Science 284, 616–618.

Marzoli, A., et al., 2004. Synchrony of the Central Atlantic magmatic province and the Triassic-Jurassic boundary climatic and biotic crisis. Geology 32, 973–976.

Marzoli, A., et al., 2011. Timing and duration of the Central Atlantic magmatic province in the Newark and Culpeper basins, eastern U.S.A. Lithos 122, 175–188.

Marzoli, A., et al., 2018. The Central Atlantic Magmatic Province (CAMP): a review. Chapter 4 in The Late Triassic World. Top. Geobiol. 46, 91–125.

Marzoli, A., et al., 2019. The Central Atlantic Magmatic Province (CAMP) in Morocco. J. Petrol. 60, 945–996.

Mattey, D.P., Carr, R.H., Wright, I.P., Pillinger, C.T., 1984. Carbon isotopes in submarine basalts. Earth Planet. Sci. Lett. 70, 196–206.

McElwain, J.C., Beerling, D.J., Woodward, F.I., 1999. Fossil plants and global warming at the Triassic-Jurassic boundary. Science 285, 1386–1390.

McGhee Jr., G.R., Sheehan, P.M., Bottjer, D.J., Droser, M.L., 2004. Ecological ranking of Phanerozoic biodiversity crises: ecological and taxonomic severities are decoupled. Palaeogeogr. Palaeoclimatol. Palaeoecol. 211, 289–297.

McHone, J.G., 2003. Volatile emissions from Central Atlantic Magmatic Province Basalts: mass assumptions and environmental consequences. In The Central Atlantic Magmatic Province. Insights from fragments of Pangea. AGU Geophys. Monogr. 136, 241–254.

McRoberts, C.A., Newton, C.R., 1995. Selective extinction among end-Triassic European bivalves. Geology 23, 102–104.

Moore, J.G., 2001. Density of basalt core from Hilo drill hole, Hawaii. J. Volcanol. Geotherm. Res. 112, 221–230.

Nomade, S., et al., 2007. Chronology of the Central Atlantic Magmatic Province: implications for the Central Atlantic rifting processes and the Triassic–Jurassic biotic crisis. Palaeogeogr. Palaeoclimatol. Palaeoecol. 244, 326–344.

Pálfy, J., Zajzon, N., 2012. Environmental changes across the Triassic–Jurassic boundary and coeval volcanism inferred from elemental geochemistry and mineralogy in the Kendlbachgraben section (Northern Calcareous Alps, Austria). Earth Planet. Sci. Lett. 335-336, 121–134.

Pálfy, J., et al., 2001. Carbon isotope anomaly and other geochemical changes at the Triassic-Jurassic boundary from a marine section in Hungary. Geology 29, 1047–1050.

Pálfy, J., et al., 2007. Triassic–Jurassic boundary events inferred from integrated stratigraphy of the Csővár section, Hungary. Palaeogeogr. Palaeoclimatol. Palaeoecol. 244, 11–33.

Panfili, G., et al., 2019. New biostratigraphic constraints show rapid emplacement of the Central Atlantic Magmatic Province (CAMP) during the end-Triassic mass extinction interval. Glob. Planet. Chang. 172, 60–68.

Paris, G., Donnadieu, Y., Beaumont, V., Fluteau, F., Goddéris, Y., 2016. Geochemical consequences of intense pulse-like degassing during the onset of the Central Atlantic Magmatic Province. Palaeogeogr. Palaeoclimatol. Palaeoecol. 441, 74–82.

Payne, J.L., Kump, L.R., 2007. Evidence for recurrent Early Triassic massive volcanism from quantitative interpretation of carbon isotope fluctuations. Earth Planet. Sci. Lett. 256, 264–277.

Plank, T., Manning, C.E., 2019. Subducting carbon. Nature 574, 343–352.

Rampino, M.R., Caldeira, K., 2005. Major perturbation of ocean chemistry and a 'Strangelove Ocean' after the end-Permian mass extinction. Terra Nova 17, 554–559.

Raup, D.M., Sepkoski Jr., J.J., 1982. Mass extinctions in the marine fossil record. Science 215, 1501–1503.

Ruhl, M., et al., 2020. On the onset of Central Atlantic Magmatic Province (CAMP) volcanism and environmental and carbon-cycle change at the Triassic–Jurassic transition (Neuquén Basin, Argentina). Earth-Sci. Rev. 208, 103229.

Schaller, M.F., Wright, J.D., Kent, D.V., 2011. Atmospheric PCO$_2$ perturbations associated with the Central Atlantic Magmatic Province. Science 331, 1404–1409.

Schaltegger, U., Guex, J., Bartolini, A., Schoene, B., Ovtcharova, M., 2008. Precise U–Pb age constraints for end-Triassic mass extinction, its correlation to volcanism and Hettangian post-extinction recovery. Earth Planet. Sci. Lett. 267, 266–275.

Schidlowski, M., 2001. Carbon isotopes as biogeochemical recorders of life over 3.8 Ga of Earth history: evolution of a concept. Precambrian Res. 106, 117–134.

Schmidt, A., et al., 2016. Selective environmental stress from sulphur emitted by continental flood basalt eruptions. Nat. Geosci. 9, 77–82.

Schoene, B., Guex, J., Bartolini, A., Schaltegger, U., Blackburn, T.J., 2010. Correlating the end-Triassic mass extinction and flood basalt volcanism at the 100 ka level. Geology 38, 387–390.

Shields, G.A., Mills, B.J.W., 2021. Evaporite weathering and deposition as a long-term climate forcing mechanism. Geology 49, 299–303.

Tanner, L.H., Lucas, S.G., Chapman, M.G., 2004. Assessing the record and causes of Late Triassic extinctions. Earth-Sci. Rev. 65, 103–139.

Tegner, C., et al., 2019. Mantle dynamics of the Central Atlantic Magmatic Province (CAMP): constraints from platinum group, gold and lithophile elements in flood basalts of Morocco. J. Petrol. 60, 1621–1652.

Todaro, S., Rigo, M., Randazzo, V., Di Stefano, P., 2018. The end-Triassic mass extinction: a new correlation between extinction events and δ^{13}C fluctuations from a Triassic-Jurassic peritidal succession in western Sicily. Sediment. Geol. 368, 105–113.

van de Schootbrugge, B., Wignall, P.B., 2016. A tale of two extinctions: converging end-Permian and end-Triassic scenarios. Geol. Mag. 153 (2), 332–354.

Walker, J.C.G., Kasting, J.F., 1992. Effects of fuel and forest conservation on future levels of atmospheric carbon dioxide. Palaeogeogr. Palaeoclimatol. Palaeoecol. 97, 151–189.

Weems, R.E., Tanner, L.H., Lucas, S.G., 2016. Synthesis and revision of the lithostratigraphic groups and formations in the Upper Permian?-Lower Jurassic Newark Supergroup of eastern North America. Stratigraphy 13, 111–153.

Wignall, P.B., 2001. Large igneous provinces and mass extinctions. Earth-Sci. Rev. 53, 1–33.

Wignall, P.B., 2015. The Worst of Times: How Life on Earth Survived Eighty Million Years of Extinctions, 224 pp. Princeton University Press, Princeton.

Wignall, P.B., Atkinson, J.W., 2020. A two-phase end-Triassic mass extinction. Earth-Sci. Rev. 208, 103282.

Wotzlaw, J.-F., et al., 2014. Towards accurate numerical calibration of the Late Triassic: high-precision U-Pb geochronology constraints on the duration of the Rhaetian. Geology 42, 571–574.

Yager, J.A., et al., 2017. Duration of and decoupling between carbon isotope excursions during the end-Triassic mass extinction and Central Atlantic Magmatic Province emplacement. Earth Planet. Sci. Lett. 473, 227–236.